ACS APPLIED MATERIALS & INTERFACES

Research Article

www.acsami.org

Kilogram-Scale Synthesis of Pd-Loaded Quintuple-Shelled Co_3O_4 Microreactors and Their Application to Ultrasensitive and Ultraselective Detection of Methylbenzenes

Ji-Wook Yoon,[†] Young Jun Hong,[†] Gi Dae Park,[†] Su-Jin Hwang,[†] Faissal Abdel-Hady,[‡] AbdulAziz A. Wazzan,[‡] Yun Chan Kang,*[,†] and Jong-Heun Lee*[,†,‡]

[†]Department of Materials Science and Engineering, Korea University, Seoul 136-713, Republic of Korea

[‡]Department of Chemical and Materials Engineering, King Abdulaziz University, Jeddah 21589, Saudi Arabia

Supporting Information

ABSTRACT: We report the kilogram-scale, simple, and cost-effective synthesis of Pd-loaded quintuple-shelled Co_3O_4 microreactors by spray drying of aqueous droplets containing cobalt nitrate, palladium nitrate, citric acid, and ethylene glycol and subsequent heat treatment. Highly viscous gel spheres containing Co and Pd salts were successfully converted into multi thin-shelled Co_3O_4 reactors uniformly loaded with Pd catalysts by the sequential combustion of carbon and decomposition of the metal salts from the outer to the inner regions during one-step heat treatment. The responses (resistance ratio) of the Pd-loaded quintuple-shelled Co_3O_4 microreactors to 5 ppm toluene and *p*-xylene were 30.8 and 64.2, respectively, and the selectivity values to toluene and *p*-xylene against ethanol interference (response ratio) were 14.5 and 30.1, respectively. The unprecedented high response and selectivity were attributed to the effective dissociation of less reactive methylbenzenes into more active smaller species assisted both by catalytic Co_3O_4 and Pd during the prolonged retention within the microreactors. Kilogram-scale preparation of noble metal-loaded multishelled microreactors and their unique gas-sensing characteristics based on a novel microreactor concept can pave a new way to design of high-performance gas sensors for practical applications.

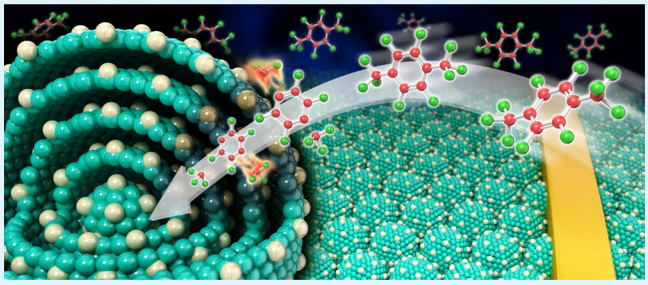

KEYWORDS: *gas sensor, Pd-loaded Co_3O_4, yolk–shell microreactor, kilogram-scale preparation, selectivity, methylbenzenes*

1. INTRODUCTION

Noble metal-loaded metal oxide materials with yolk–shell structures have been receiving tremendous attention in the fields of catalysts, microreactors, and gas sensors because of their unique nanoarchitectures, which facilitate rapid mass transfer throughout the entire nanostructure and high controllability of chemical reactions within the semipermeable shells.[1−6] Thus, far, heterostructured yolk–shell materials with the configuration noble metal@void@metal oxide prepared by hydrothermal/solvothermal reactions have been explored as catalysts and gas sensors.[7−11] The performance of catalysts and gas sensors can be further improved or tuned by uniform loading of nanoscale noble metal catalysts such as Pd, Ag, Rh, Au, and Pt on metal oxide nanostructures.[6,11−16] However, most chemical routes based on impregnation and sacrificial templates require prolonged multistep procedures for loading catalysts onto multiple shells and coating the thin shell layers. Such procedures often lead to significant loss of expensive Pd-source materials during processing and the aggregation of metal catalyst nanoparticles, which hampers cost-effective mass production and deteriorates the performance of microreactor-based devices. Therefore, the simple, large-scale, and reproducible synthesis of yolk–shell oxides uniformly loaded with noble metal catalysts is not only important, it can also pave the way for various new applications.

Recently, we prepared SnO_2 yolk–shell nanostructures uniformly loaded with Pd by one-pot spray pyrolysis of aqueous droplets containing tin oxalate, palladium (II) nitrate hydrate, and sucrose.[12] The synthetic strategy was confirmed by preparation of Ag-loaded SnO_2 yolk–shell nanostructures.[13] SnO_2 yolk–shell nanostructures loaded with Pd[12] and Ag[13] showed unusually high selectivity to methylbenzene and H_2S, respectively, which demonstrates a new strategy for designing high-performance gas sensors based on a novel microreactor concept. However, it is challenging to achieve the kilogram-scale preparation of metal-loaded oxide yolk–shell nanostructures using spray pyrolysis. The spray drying process, on the other hand, is known to be cost-effective, with high throughput of powders with a spherical morphology. The production efficiency of the spray-drying process is several tens of times higher than that of similar-scale spray pyrolysis processes. Indeed, one of the present authors successfully demonstrated

Received: January 23, 2015
Accepted: March 25, 2015
Published: March 25, 2015

DOI: 10.1021/acsami.5b00706
ACS Appl. Mater. Interfaces 2015, 7, 7717−7723

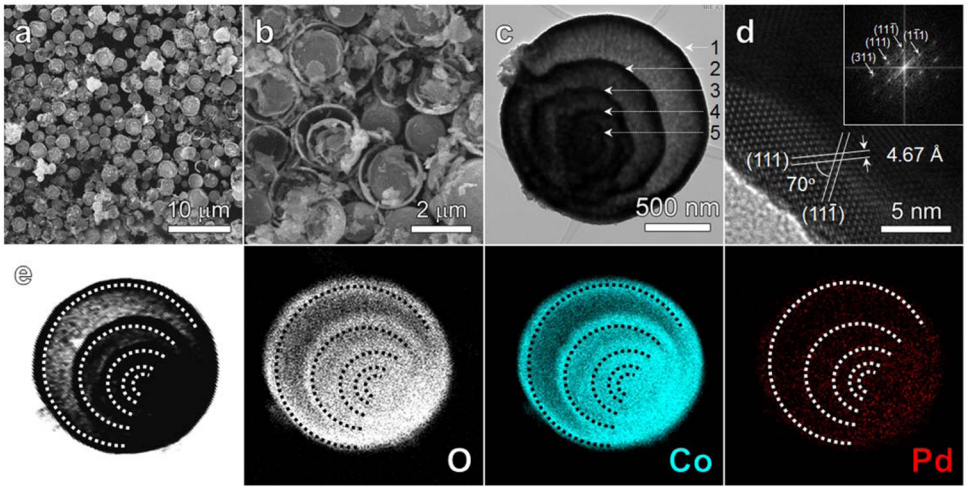

Figure 1. SEM and TEM images of Pd–Co_3O_4-MRs: (a, b) SEM images; (c) TEM image to show multiple-shelled yolk–shell structures; (d) high-resolution lattice image of shells and fast Fourier transformation pattern; (e) TEM elemental mapping images.

the large-scale production of pure yolk–shell oxide spheres by spray drying and subsequent heat treatment.[17,18] However, noble metal-loaded yolk–shell materials have never been prepared by spray drying.

In this study, for the first time, the kilogram-scale production of noble metal-loaded yolk–shell materials is introduced. The precursor powders directly prepared by large-scale spray drying (~1 kg per day) from an aqueous spray solution of metal salts were transformed into noble metal-loaded metal oxide yolk–shell microspheres simply by heat treatment at low temperatures below 300 °C under air atmosphere. Both cobalt oxide (Co_3O_4) and Pd are known to promote the oxidation of various volatile organic compounds (VOCs), and thus they can be considered good candidate materials for high-performance sensors capable of detecting indoor VOC pollutants in a selective manner.[19−24] Indeed, we previously demonstrated the selective detection of methylbenzenes using Pd-loaded Co_3O_4 hierarchical nanostructures prepared by a solvothermal reaction,[25] although this method was not convenient for preparing sensing materials on a large scale. Accordingly, in the present study, Co_3O_4 yolk–shell nanostructures uniformly loaded with Pd catalysts were prepared on a large scale and their gas-sensing characteristics were investigated. The selectivity of the Pd-loaded Co_3O_4 yolk–shell nanostructures to methylbenzenes was significantly higher than those of Pd-loaded Co_3O_4 nanoparticles prepared by flame spray pyrolysis and Co_3O_4 hierarchical nanostructures previously reported.[25] The ultrasensitive and ultraselective detection of methylbenzenes by Pd-loaded Co_3O_4 yolk–shell nanostructures is discussed in terms of the gas-reforming reaction within unique catalyst-loaded microreactors.

2. EXPERIMENTAL SECTION

Sample Preparation. The spray drying system applied in the preparation of the precursor powders for the Pd-loaded quintuple-shelled Co_3O_4 microreactors is shown in Figure S1 in the Supporting Information. The content of Pd in the microreactors was fixed at 0.3 wt %. The temperatures at the inlet and outlet of the spray dryer were 300 and 130 °C, respectively. A two-fluid nozzle was used as an atomizer, and the atomization pressure was fixed at 2.4 bar (270 kPa). The spray solution was prepared by dissolving cobalt nitrate hexahydrate [$Co(NO_3)_2{\cdot}6H_2O$, Junsei Co., Ltd., Japan], palladium nitrate [$Pd(NO_3)_2$, Aldrich Chemical Co., Ltd., USA], citric acid (CA) [$C_6H_8O_7{\cdot}H_2O$, Samchun Chemical Co., Ltd., Korea], and ethylene glycol (EG) [$C_2H_6O_2$, Samchun Chemical Co., Ltd., Korea] in distilled water. The solution concentration of the cobalt component was 0.15 M and those of the CA and EG components were each 0.1 M. The precursor particles obtained by spray drying were converted to Pd-loaded quintuple-shelled Co_3O_4 microreactors (referred to as "Pd-Co_3O_4-MRs") by heat treatment at 300 °C for 3 h (heating rate of 10 °C min^{-1}) in air. In order to compare the gas-sensing characteristics, Pd-loaded Co_3O_4 nanopowders (referred to as "Pd-Co_3O_4-NPs") were prepared by flame spray pyrolysis of a homogeneous solution containing cobalt nitrate hexahydrate (0.15 M) and palladium nitrate (0.3 wt %) in distilled water (Figure S2 in the Supporting Information). The detailed experimental setup for the flame spray pyrolysis is described elsewhere.[26,27] The flow rates of the fuel, oxidizer, and carrier gas were 5, 40, and 10 L min^{-1}, respectively.

Characterization. The phases of the powders were investigated using X-ray diffraction (XRD, Rigaku DMAX-33). Field-emission scanning electron microscopy (FE-SEM, Hitachi S-4800) and high-resolution transmission electron microscopy (HR-TEM, JEOL JEM-2100F) were used to observe the morphologies of the powders. The decomposition characteristics of the precursor powders were studied using thermogravimetric analysis (TGA, SDT Q600), which was performed in air at a heating rate of 10 °C min^{-1}. The specific surface areas were calculated using Brunauer–Emmett–Teller (BET) analysis of the nitrogen adsorption measurements (TriStar 3000, Micro-electrics). The chemical state of the Pd-loaded quintuple-shelled Co_3O_4 microreactors was analyzed by X-ray photoelectron spectroscopy (XPS, XTOOL, ULVAC-PHI). The elemental compositions of the powders were investigated using an inductively coupled plasma-optical emission spectrometer (ICP-OES, ICAP 6000, Thermo Scientific).

Gas-Sensing Characteristics. The prepared powders were dispersed in distilled water and the slurry was drop-coated on an alumina substrate (size: 1.5 × 1.5 mm^2) with two Au electrodes on the top surface and a microheater on the bottom surface. Prior to the measurements, the sensor was heated to 350 °C for 2 h to remove any hydroxyl contaminants and to stabilize the sensor. The R_g/R_a and R_a/R_g (R_g, resistance in the analytic gas; R_a, resistance in air) ratios were used to determine the gas responses (S) to oxidizing and reducing gases, respectively. The gas responses to 5 ppm toluene, *p*-xylene, benzene, ethanol, ammonia, formaldehyde, carbon monoxide, hydrogen, and nitrogen dioxide were measured by switching the gas atmospheres at 200–300 °C. The detailed experimental setup for measuring the gas-sensing characteristics is described elsewhere.[28]

DOI: 10.1021/acsami.5b00706
ACS Appl. Mater. Interfaces 2015, 7, 7717−7723

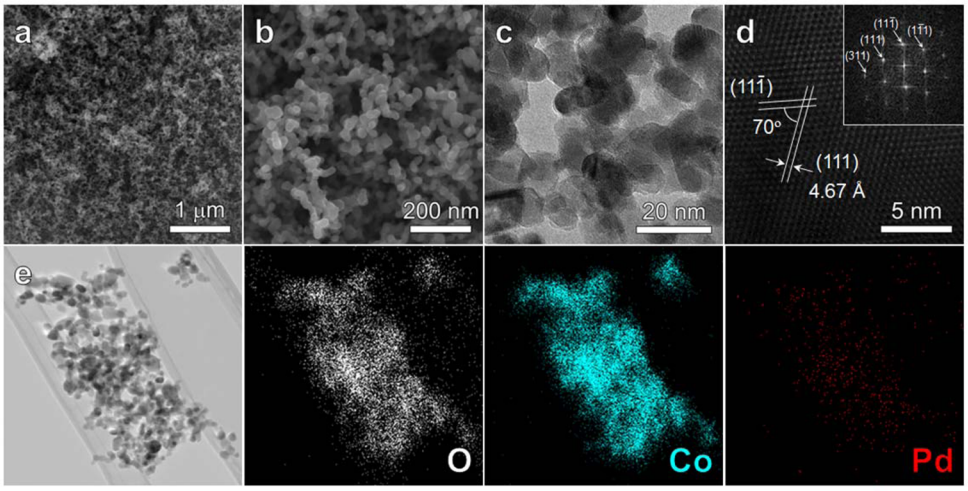

Figure 2. SEM and TEM images of Pd-Co_3O_4-NPs: (a, b) SEM images; (c) TEM image; (d) high-resolution lattice image and fast Fourier transformation pattern; (e) TEM elemental mapping images.

3. RESULTS AND DISCUSSION

Composition, Structural, and Morphological Properties. The as-prepared precursor powder particles spray-dried from droplets containing cobalt and palladium salts, citric acid, and ethylene glycol had spherical shapes and dense structures (Figure S3 in the Supporting Information). Decomposition of the Co and Pd salts as well as carbon components did not occur completely during the spray drying process because of the short residence time within the spray-drying chamber at low temperature below 300 °C. The esterification reaction between the carboxyl groups in the citric acid and the hydroxyl groups in the ethylene glycol during the spray drying process resulted in a highly viscous gel consisting of a three-dimensional organic polymer network. This viscous gel promoted volume precipitation and resulted in the formation of powder particles with spherical shapes and dense morphologies. The XRD pattern (Figure S4 in the Supporting Information) shows the amorphous characteristics of the spray-dried powder particles. The decomposition of the spray-dried spheres occurred in four steps (Figure S5 in the Supporting Information). The first weight loss below 100 °C is ascribed to the evaporation of the adsorbed water molecules. The steep weight loss observed at ~100 °C is attributed to the burning of low-molecular-weight cobalt nitrate, which did not participate in the esterification reaction. The gradual weight loss between 100 and 270 °C emanated from the decomposition of the cobalt citrate-nitrate complex and carbonization of the organic polymers formed by the esterification reaction. The final weight loss between 270 and 380 °C is ascribed to the burning of the carbon component in air.

The morphologies and elemental mapping images of the quintuple-shelled Pd-Co_3O_4-MRs are shown in Figure 1. The spherical morphology was maintained after heat treatment of the precursor powders at 300 °C for 3 h in an air atmosphere (Figure 1a). The multishelled yolk−shell structures are clearly observed from the broken spheres (Figure 1b). The TEM image (Figure 1c) confirms the yolk−shell structure of the quintuple-shelled Pd-Co_3O_4-MRs. The shell number of the microsphere was 5 (Figure 1c). The multishelled morphology is a result of the following reactions: (1) the formation of Pd-Co-C composite spheres by carbonization of the polymeric component and decomposition of Co and Pd salts, (2) the combustion of carbon and decomposition/oxidation of the outer part of Pd-Co-C sphere into Pd-Co_3O_4 outermost shell and subsequent contraction of the inner Pd-Co-C spheres, (3) repeated combustion of carbon and decomposition/oxidation of Pd-Co-C sphere at outer part of composite spheres and subsequent contraction of the inner Pd-Co-C composite spheres. Thus, the quintuple-shelled Pd-Co_3O_4-MRs were prepared by repeating the combustion and contraction processes five times during heat treatment. The high-resolution lattice fringes and fast Fourier transformation pattern (Figure 1d) confirm that the phase of the quintuple shells is Co_3O_4. The elemental mapping (Figure 1e) shows the uniform distribution of Co and Pd components throughout the quintuple-shelled Pd-Co_3O_4-MRs, indicating no phase separation of Pd and Co components during spray drying and heat treatment. This can be attributed to the role of citric acid as a chelating agent, which minimized the phase separation of the Co and Pd components.

To investigate the role of the quintuple-shelled microreactor morphology on the gas-sensing characteristics, we prepared Pd-Co_3O_4-NPs by one-pot flame spray pyrolysis for comparison. The morphologies and elemental mapping images of the Pd-Co_3O_4-NPs are shown in Figure 2. The nanoparticles, which were 10−20 nm in size, were softly aggregated (Figure 2a−c). During flame spray pyrolysis, micron-sized powders were formed first by the drying and decomposition of droplets at the entrance of the high-temperature diffusion flame. The micrometer-sized Co_3O_4-Pd composite powders were then evaporated into Co_3O_4 and Pd metal vapors within the high-temperature diffusion flame (>2500 °C). The Co_3O_4-Pd composite nanoparticles were then formed from the evaporated vapors by nucleation, growth, coagulation, and coalescence processes. The mean size of 100 nanoparticles from the TEM image was 17.0 ± 7.0 nm. In the high-resolution image (Figure 2d), two lattice planes with the same interplanar distance of 4.67 Å and an angle of 70° were observed, which correspond to the (111) and (11$\bar{1}$) planes of the Co_3O_4 spinel structure. The elemental mapping images (Figure 2e) show the uniform distribution of Pd completely covering the crystalline Co_3O_4 nanoparticles.

Both the quintuple-shelled Pd-Co_3O_4-MRs and the Pd-Co_3O_4-NPs were identified as the Co_3O_4 spinel phase (JCPDS

DOI: 10.1021/acsami.5b00706
ACS Appl. Mater. Interfaces 2015, 7, 7717−7723

#42−1467) (Figure 3). No Pd-related second phase was observed, probably owing to the low detection limit of X-ray

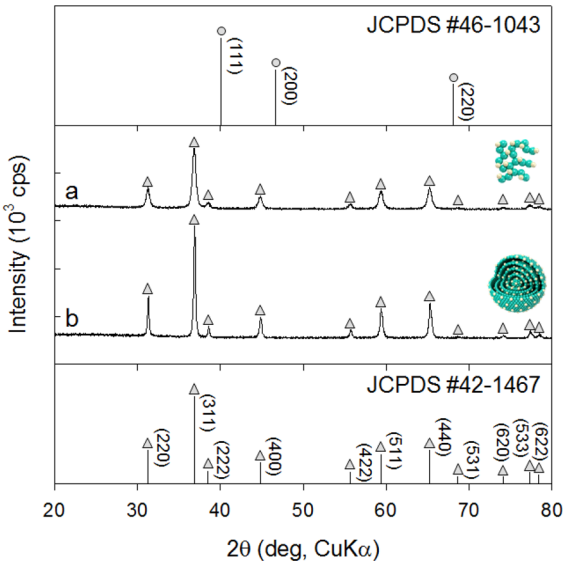

Figure 3. X-ray diffraction patterns (XRD) of the (a) Pd-Co_3O_4-NPs and (b) Pd-Co_3O_4-MRs.

diffraction. XPS analysis was carried out to confirm the oxidation state of Pd in the quintuple-shelled Pd-Co_3O_4-MRs (Figure S6 in the Supporting Information). Because the Pd characteristic peaks for Pd $3d_{3/2}$ and $3d_{5/2}$ in the 0.3 wt % Pd-loaded powders could not be observed, probably because of the low concentration of Pd below the detection limits of XPS, 5.0 wt % Pd-loaded quintuple-shelled Co_3O_4 microreactors were analyzed. The Co 2p XPS spectrum was resolved into Co-related peaks and a satellite peak (Figure S6b in the Supporting Information). The binding energies of the deconvoluted peaks in the spectrum of Co $2p_{3/2}$ were 779.9 eV (blue) and 780.1 eV (green), which corresponded to Co^{3+} and Co^{2+}, respectively, of the Co_3O_4 phase.[29,30] Pd $2d_{3/2}$ and Pd $3d_{5/2}$ peaks were found at 342.2 and 336.9 eV, respectively, indicating that the oxidation state of Pd was Pd^{2+} (Figure S6c in the Supporting Information).[30,31] The presence of PdO was cross-checked by the O 1s spectrum (Figure S6d in the Supporting Information). The lattice oxygen-related peak remained nonsymmetric, even after removing the effect of water adsorbents such as hydroxyl (green) and water (gray) molecules. This indicates that there were two types of bonding, O−Co and O−Pd. The binding energies of O−Co in Co_3O_4 and O−Pd in PdO were 530.0 and 530.1 eV, respectively, values that are consistent with those in previous reports.[30,32]

The pore-size distributions of the quintuple-shelled Pd-Co_3O_4-MRs and Pd-Co_3O_4-NPs were investigated by nitrogen isothermal adsorption (Figure 4). The BET surface areas of the Pd-Co_3O_4-NPs and the quintuple-shelled Pd-Co_3O_4-MRs were 19.0 and 10.0 $m^2\ g^{-1}$, respectively (Figures 4a and c). The quintuple-shelled Pd-Co_3O_4-MRs exhibited clear mesopores with a mean size of 25 nm (Figure 4d), whereas the Pd-Co_3O_4-NPs had dense structures with a lower interparticle pore volume (Figure 4b).

Gas-Sensing Characteristics. The gas-sensing characteristics of the quintuple-shelled Pd-Co_3O_4-MRs and Pd-Co_3O_4-NPs are shown in Figure 5. Considering that most oxide semiconductor gas sensors show a high response to ethanol, the

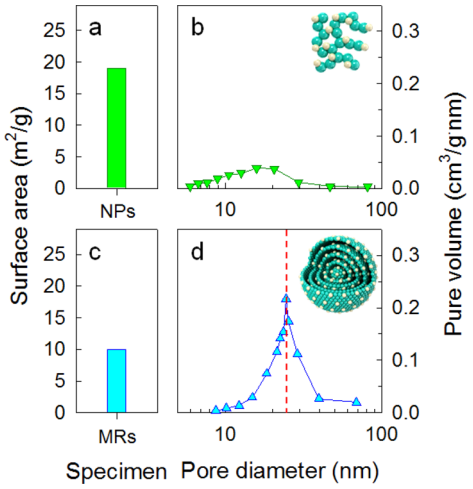

Figure 4. BET surface area and pore-size distribution of the (a, b) Pd-Co_3O_4-NPs and (c, d) Pd-Co_3O_4-MRs.

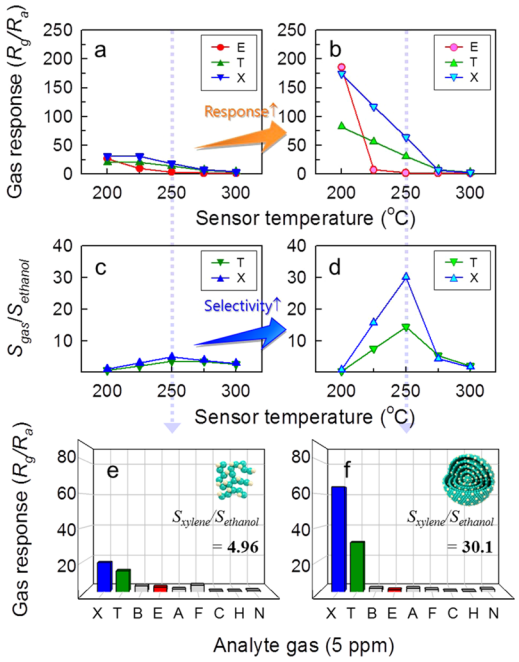

Figure 5. Gas responses (R_g/R_a) and selectivity ($S_{gas}/S_{ethanol}$; S_{gas}, gas responses to 5 ppm xylene and toluene; $S_{ethanol}$, gas response to 5 ppm ethanol) of the (a, c) Pd-Co_3O_4-NPs and (b, d) Pd-Co_3O_4-MRs. Gas responses (R_g/R_a) of the (e) Pd-Co_3O_4-NPs and (f) Pd-Co_3O_4-MRs to 5 ppm *p*-xylene (X), toluene (T), benzene (B), ethanol (E), ammonia (A), formaldehyde (F), carbon monoxide (C), hydrogen (H), and nitrogen monoxide (N).

responses ($S = R_g/R_a$; R_g, resistance in the analytic gas; R_a, resistance in air) to *p*-xylene and toluene were compared to the cross-responses to ethanol (Figures 5a, b). The values of selectivity toward *p*-xylene and toluene against interference from ethanol ($S_{xylene}/S_{ethanol}$ and $S_{toluene}/S_{ethanol}$) were as high as 30.1 and 14.5, respectively, at 250 °C in the Pd−Co_3O_4-MRs, whereas those of the Pd−Co_3O_4−NPs were 3.6 and 5.0, respectively (Figure 5c, d). The quintuple-shelled Pd-Co_3O_4-MRs showed ultrahigh and ultraselective responses to 5 ppm *p*-xylene (R_g/R_a = 64.2) and toluene (R_g/R_a = 30.8), with negligible cross-responses to 5 ppm ethanol, benzene, ammonia, formaldehyde, carbon monoxide, hydrogen, and

DOI: 10.1021/acsami.5b00706
ACS Appl. Mater. Interfaces 2015, 7, 7717−7723

nitrogen monoxide (R_g/R_a or R_a/R_g = 1.2−3.1) at 250 °C (Figure 5f). The ultrahigh response and selectivity to methylbenzenes of the quintuple-shelled Pd-Co_3O_4-MRs were also observed at 225 °C (Figure S7 in the Supporting Information). In contrast, the selectivity values to methylbenzenes were relatively low in the Pd−Co_3O_4−NPs at 225 and 250 °C (Figures 5e and Figure S7 in the Supporting Information). The 90% response and recovery times (τ_{res} and τ_{recov}), i.e., the times needed to reach 90% resistance variation upon exposure to 5 ppm methylbenzenes and air, were calculated from the sensing transients at 200−300 °C (Figure 6). The τ_{res} values of the quintuple-shelled Pd-Co_3O_4-MRs to *p*-

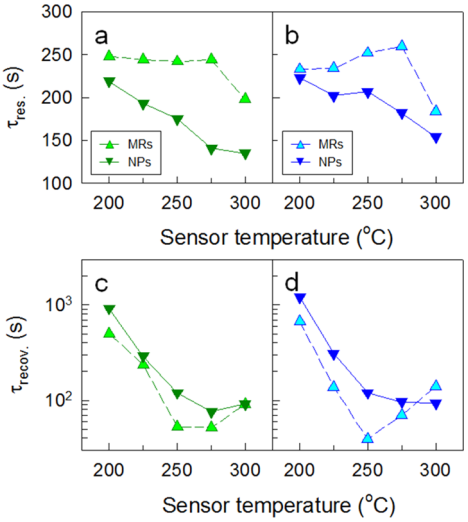

Figure 6. 90% response times (τ_{res}) of the Pd-Co_3O_4-MRs and Pd-Co_3O_4-NPs to (a) xylene and (b) toluene at 200−300 °C and 90% recovery times (τ_{recov}) to (c) xylene and (d) toluene at 200−300 °C.

xylene and toluene were higher in comparison to those of the Pd-Co_3O_4-NPs (Figures 6a, b) for all sensor temperatures, whereas the τ_{recov} values showed the opposite tendencies at 200−275 °C (Figure 6c, d). The higher τ_{res} values of the quintuple-shelled Pd-Co_3O_4-MRs will be discussed in a later section.

Sensitive and selective detection of methylbenzenes regardless of morphological variation in Pd-loaded Co_3O_4 nanostructures can be attributed to the characteristics of sensing and catalyst materials. P-type metal oxide semiconductors such as Co_3O_4, Cr_2O_3, NiO, and CuO, which have abundant oxygen adsorption and multivalence characteristics, are known to be good catalysts for oxidizing various VOCs.[33] The Co_3O_4 is an excellent catalyst for methylbenzenes, and it has been used as a gas sensor to detect xylene and toluene.[34] Pd is a representative catalyst that enhances the gas response or selectivity by reducing the charge carrier concentration of the host metal oxide through the formation of PdO (Pd^{2+}) in air atmosphere (electronic sensitization) or by promoting the catalytic oxidation of the analyte gases (chemical sensitization).[35] The sensor resistance in air (R_a) of the Pd-loaded Co_3O_4 nanoparticles was ∼7 kΩ at 250 °C, which was similar to the 8 kΩ value of undoped Co_3O_4 nanoparticles with the same morphology (Figure S8 in the Supporting Information). This indicates that the enhanced gas response is attributed to the chemical sensitization rather than electronic sensitization by Pd loading. Thus, the high response and selectivity to methylbenzenes in the present two sensors can be ascribed to the synergetic catalytic effects of Co_3O_4 and Pd. This is supported by our previous investigation in which we reported the high response and selectivity to methylbenzenes of Pd-loaded Co_3O_4 hollow hierarchical nanostructures prepared by a small-scale hydrothermal reaction.[25]

The gas responses of the quintuple-shelled Pd-Co_3O_4-MRs were significantly high as compared to those of the Pd-loaded Co_3O_4 agglomerated nanoparticles (Figures 5a and b). Co_3O_4 forms a charge (hole) accumulation layer near the surface of the primary particles by the adsorption of negatively charged oxygen. The gas response can significantly increase when the primary particle size is comparable to twice the thickness of the hole accumulation layer. Thus, smaller primary particles are more favorable for enhancing the gas response. The primary particle size of the Pd-Co_3O_4-NPs determined by Scherrer's eq (23.1 ± 8.1 nm) is smaller than that of the quintuple-shelled Pd−Co_3O_4-MRs (42.4 ± 6.8 nm), and the BET surface area of the Pd-Co_3O_4-NPs (19.0 m^2g^{-1}) is approximately twice that of the quintuple-shelled Pd-Co_3O_4-MRs (10.0 m^2 g^{-1}). The higher response of the quintuple-shelled Pd-Co_3O_4-MRs to methylbenzenes despite their larger particle size and lower BET surface area strongly indicates the importance of the yolk−shell morphology with abundant pores in the gas-sensing reaction. Generally, oxide nanoparticles form large agglomerates as a result of van der Waals attraction. When agglomerates are large and dense, the gas-sensing reaction occurs mostly at the outer part, while the inner part of the agglomerates remains inactive, leading to a relatively low gas response. Thus, the low gas response of the Pd-Co_3O_4-NPs can be attributed to the decrease of gas accessibility because of agglomeration. In the Pd-Co_3O_4-MRs, the gas response is primarily determined by the outermost shell. A thin and semipermeable outermost shell will provide more effective hole accumulation from both the inner and outer parts of the shells as a result of high gas accessibility, which enhances the gas response.

The unprecedented high selectivity to methylbenzenes in the quintuple-shelled Pd-Co_3O_4-MRs can be also understood in relation to the unique microreactor morphology. In the Pd-Co_3O_4-NPs, the methylbenzenes are dissociated or partially oxidized into more active smaller species near the surfaces of the agglomerates. Thus, some of the products take part in the gas-sensing reaction, whereas the remaining products diffuse out to the ambient atmosphere. In contrast, the methylbenzenes that diffused into the inner part of the quintuple-shelled Pd-Co_3O_4-MRs through the thin and semipermeable shells can remain within the microreactors for an extended period of time. Moreover, the Pd-Co_3O_4 yolk parts and the inner surface of the outermost Pd-Co_3O_4 shell will promote the dissociation or partial oxidation of methylbenzenes into more reactive smaller species.[36] This can enhance the gas response to methylbenzenes, which is analogous to the improved response to larger and less reactive gas molecules such as benzene derivatives by the prolonged retention of the analyte gas within Pd-containing nanovolumes underneath WO_3 thin films[37] or within Pd-SnO_2 yolk−shell nanostructures.[12] The longer τ_{res} values of the quintuple-shelled Pd-Co_3O_4-MRs as compared to those of the Pd-Co_3O_4-NPs (Figure 6) in the present study strongly support the reformation of less reactive benzene derivatives into more active species during the retention of the analyte gas. That is, the catalyst-loaded Co_3O_4 microreactors with multiple shells and yolk in the present study can be used a unique strategy to promote the reformation of methylbenzenes into more active species for gas sensing. The decrease of

DOI: 10.1021/acsami.5b00706
ACS Appl. Mater. Interfaces 2015, 7, 7717−7723

ethanol response (from 185.3 to 7.4) at 200−250 °C in the quintuple-shelled Pd-Co_3O_4-MRs is significantly higher than that in the Pd-Co_3O_4-NPs (from 26.7 to 9.8) at the same temperature regime (Figures 5a, b). The abrupt decrease of response to C_2H_5OH of the quintuple-shelled Pd-Co_3O_4-MRs at >225 °C can be explained by the effective oxidation of C_2H_5OH into less reactive or nonreactive CO_2(g) and H_2O(g) during the retention of gas within the microreactor.

The dynamic sensing transients of the quintuple-shelled Pd-Co_3O_4-MRs to 0.25−5 ppm *p*-xylene and toluene were measured at 250 °C (Figure S9 in the Supporting Information). Stable recovery after sensing different concentrations of methylbenzenes was observed. The sensor showed high responses to 0.25 ppm *p*-xylene (R_g/R_a = 1.4) and toluene (R_g/R_a = 1.6), demonstrating the detection of sub-ppm-level methylbenzenes.

Typical concentrations of methylbenzenes in unpolluted indoor air are in the sub-ppm level. Health Canada recommended 4 (8 h TWA (time weighted average, the average concentration of contaminants over a specified time period)) and 0.6 ppm (24 h TWA) as the residential maximum exposure limits for methylbenzenes.[38] Accordingly, the sub-ppm-level detection of methylbenzenes is essential. However, the responses to less reactive methylbenzenes in most n-type oxide semiconductor gas sensors are significantly lower than those to reactive and ubiquitous indoor pollutant such as ethanol.[39−41] Accordingly, the selective detection of indoor methylbenzenes with negligible cross-response of ethanol remains a challenging issue. The S_{xylene} and $S_{xylene}/S_{ethanol}$ of the quintuple-shelled Pd-Co_3O_4-MRs in the present study were ultrahigh as 61.2 and 30.1, respectively, values that are significantly higher than those of Pd-loaded SnO_2 yolk−shell nanostructures ($S_{xylene} \approx 17.4$ and $S_{xylene}/S_{ethanol} \approx 2.9$)[12] and Cr-doped Co_3O_4 nanorods ($S_{xylene} \approx 11.0$ and $S_{xylene}/S_{ethanol} = \sim 6.1$).[34] Our group[25] reported that Pd-loaded Co_3O_4 hierarchical nanostructures exhibited high responses to 5 ppm xylene and toluene (S_{xylene} = 186, $S_{toluene}$ = 124), as well as high selectivity to methylbenzenes ($S_{xylene}/S_{ethanol}$ = 7.7 and $S_{toluene}/S_{ethanol}$ = 5.2) at 275 °C. This clearly shows that both Co_3O_4 and Pd are important catalysts for enhancing the sensing of methylbenzenes. In particular, it should be noted that the selectivity values to xylene and toluene of the present Pd−Co_3O_4-MRs ($S_{xylene}/S_{ethanol}$ = 30.1 and $S_{toluene}/S_{ethanol}$ = 14.5) are 3.98 and 2.81 times higher, respectively, than those of the Pd-loaded Co_3O_4 hierarchical nanostructures, even though the gas response is slightly lower. This means that the ultimate level of selectivity to methylbenzenes can be accomplished by the unique design of microreactors with two different catalytic materials, Co_3O_4 and Pd. Moreover, the kilogram-scale production of sensing materials via a facile one-pot spray drying reaction facilitates the development of practical applications. Therefore, the control or tuning of a gas-reforming/oxidation reaction within a catalyst-loaded microreactor prepared by large-scale spray drying can provide a new and general strategy for designing highly selective and sensitive gas sensors.

4. CONCLUSION

Quintuple-shelled Co_3O_4 microreactors uniformly loaded with Pd nanoparticles were prepared for the first time on a kilogram-scale using a facile spray-drying method and low-temperature heat treatment, and their gas-sensing characteristics were investigated. The Pd-loaded quintuple-shelled Co_3O_4 microreactors showed ultrahigh response ($S_{toluene}$ = 30.8 and S_{xylene} = 64.2) and ultrahigh selectivity ($S_{toluene}/S_{ethanol}$ = 14.5 and $S_{xylene}/S_{ethanol}$ = 30.1) to 5 ppm methylbenzenes with negligible cross-responses to ethanol, benzene, ammonia, formaldehyde, carbon monoxide, hydrogen, and nitrogen monoxide. The unique gas-sensing characteristics of the Pd-loaded quintuple-shelled Co_3O_4 microreactors were attributed to the effective dissociation of less reactive methylbenzenes into smaller and more active gases owing to the prolonged retention of methylbenzenes within the semipermeable Pd-Co_3O_4 shells assisted by highly catalytic Co_3O_4 and Pd. These microreactors are thus useful for monitoring representative indoor pollutants. Kilogram-scale preparation of multiple yolk−shell spheres uniformly loaded with metal catalysts can provide a new and general strategy for designing high-performance gas sensors for practical applications.

■ ASSOCIATED CONTENT

Supporting Information

Experimental setups of spray drying and flame spray pyrolysis processes; SEM images, X-ray diffraction patterns, and thermogravimetric analysis of precursor powders prepared by a spray-drying process; X-ray photoelectron spectroscopy results of 5 wt % Pd-loaded quintuple-shelled Co_3O_4 microreactors; gas responses of Pd-loaded Co_3O_4 nanoparticles and Pd-loaded quintuple-shelled Co_3O_4 microreactors to 5 ppm *p*-xylene, toluene, benzene, ethanol, ammonia, formaldehyde, carbon monoxide, hydrogen, and nitrogen monoxide at 225, 250, and 275 °C; gas-sensing transients of Pd-loaded quintuple-shelled Co_3O_4 microreactors, Pd-loaded Co_3O_4 nanoparticles, and pure Co_3O_4 nanoparticles to 5 ppm ethanol, toluene, and *p*-xylene at 250 °C; gas-sensing transients and gas responses of Pd-loaded quintuple-shelled Co_3O_4 microreactors to *p*-xylene and toluene as a function of concentration. This material is available free of charge via the Internet at http://pubs.acs.org.

■ AUTHOR INFORMATION

Corresponding Authors

*E-mail: yckang@korea.ac.kr.

*E-mail: jongheun@korea.ac.kr. Fax: +82-2-928-3584. Tel: +82-2-3290-3282.

Notes

The authors declare no competing financial interest.

■ ACKNOWLEDGMENTS

This work is supported by the Deanship of Scientific Research (DSR), King Abdulaziz University (KAU), under Grant 2-135-36-HiCi, and a National Research Foundation of Korea (NRF) grant funded by the Korea Government (MEST) (No. 2013R1A2A1A01006545). The authors, therefore, acknowledge the technical and financial support of KAU and MEST.

■ REFERENCES

(1) Yin, Y.; Rioux, R. M.; Erdonmez, C. K.; Hughes, S.; Somorjai, G. A.; Alivisatos, A. P. Formation of Hollow Nanocrystals Through the Nanoscale Kirkendall Effect. *Science* **2004**, *304*, 711−714.

(2) Zhao, Y.; Jiang, L. Hollow Micro/Nanomaterials with Multilevel Interior Structures. *Adv. Mater.* **2009**, *21*, 3621−3638.

(3) Lou, X. W.; Archer, L. A.; Yang, Z. Hollow Micro-/Nanostructures: Synthesis and Applications. *Adv. Mater.* **2008**, *20*, 3987−4019.

DOI: 10.1021/acsami.5b00706
ACS Appl. Mater. Interfaces 2015, 7, 7717−7723

(4) Liu, B.; Yu, S.; Wang, Q.; Hu, W.; Jing, P.; Liu, Y.; Jia, W.; Liu, Y.; Zhang, J. Hollow Mesoporous Ceria Nanoreactors with Enhanced Activity and Stability for Catalytic Application. *Chem. Commun.* **2013**, *49*, 3757−3759.
(5) Liu, J.; Qiao, S. Z.; Chen, J. S.; Lou, X. W. Yolk/Shell Nanoparticles: New Platforms for Nanoreactors, Drug delivery and Lithium-ion Batteries. *Chem. Commun.* **2011**, *47*, 12578−12591.
(6) Kim, H.-J.; Choi, K.-I.; Pan, A.; Kim, I.-D.; Kim, H.-R.; Kim, K.-M.; Na, C. W.; Cao, G.; Lee, J.-H. Template-Free Solvothermal Synthesis of Hollow Hematite Spheres and Their Applications in Gas Sensors and Li-Ion Batteries. *J. Mater. Chem.* **2011**, *21*, 6549−6555.
(7) Lee, J.; Park, J. C.; Song, H. A Nanoreactor Framework of a Au@SiO_2 Yolk/Shell Structure for Catalytic Reduction of *p*-Nitrophenol. *Adv. Mater.* **2008**, *21*, 1523−1528.
(8) Zhang, N.; Liu, S.; Xu, Y.-J. Recent Progress on Metal Core@Semiconductor Shell Nanocomposites as a Promising Type of Photocatalyst. *Nanoscale* **2012**, *4*, 2227−2238.
(9) Li, G.; Tang, Z. Noble Metal Nanoparticle@Metal Oxide Core/Yolk-Shell Nanostructures as Catalyst: Recent Progress and Perspective. *Nanoscale* **2014**, *6*, 3995−4011.
(10) Wang, L.; Dou, H.; Lou, Z.; Zhang, T. Encapsulated Nanoreactors (Au@SnO_2): a New Sensing Material for Chemical Sensors. *Nanoscale* **2013**, *5*, 2686−2691.
(11) Rai, P.; Yoon, J.-W.; Jeong, H.-M.; Hwang, S.-J.; Kwak, C.-H.; Lee, J.-H. Design of Highly Sensitive and Selective Au@NiO Yolk-Shell Nanoreactors for Gas Sensor Applications. *Nanoscale* **2014**, *6*, 8292−8299.
(12) Hong, Y. J.; Yoon, J.-W.; Lee, J.-H.; Kang, Y. C. One-pot Synthesis of Pd-Loaded SnO_2 Yolk-shell Nanostructures for Ultra-selective Methylbenzene Sensors. *Chem.—Eur. J.* **2014**, *20*, 2737−2741.
(13) Yoon, J.-W.; Hong, Y. J.; Kang, Y. C.; Lee, J.-H. High Performance Chemiresistive H_2S Sensors Using Ag-Loaded SnO_2 Yolk-Shell Nanostructures. *RSC Adv.* **2014**, *4*, 16067−16074.
(14) Shin, J.; Choi, S.-J.; Lee, I.; Youn, D.-Y.; Park, C. O.; Lee, J.-H.; Tuller, H. L.; Kim, I.-D. Thin-Wall Assembled SnO_2 Fibers Functionalized by Catalytic Pt Nanoparticles and Their Superior Exhaled-Breath-Sensing Properties for the Diagnosis of Diabetes. *Adv. Funct. Mater.* **2013**, *23*, 2357−2367.
(15) Kim, S.-J.; Hwang, I.-S.; Na, C. W.; Kim, I.-D.; Kang, Y. C.; Lee, J.-H. Ultrasensitive and Selective C_2H_5OH Sensors Using Rh-Loaded In_2O_3 Hollow Spheres. *J. Mater. Chem.* **2011**, *21*, 18560−18567.
(16) Cho, N. G.; Woo, H.-S.; Lee, J.-H.; Kim, I.-D. Thin-Walled NiO Tubes Functionalized with Catalytic Pd for Highly Selective C_2H_5OH Sensors Using Electrospun Fibers as a Sacrificial Template. *Chem. Commun.* **2011**, *47*, 11300−11302.
(17) Park, G. D.; Lee, J.-H.; Lee, J.-K.; Kang, Y. C. Effect of Esterification Reaction of Citric Acid and Ethylene Glycol on the Formation of Multi-Shelled Cobalt Oxide Powders with Superior Electrochemical Properties. *Nano Res.* **2014**, *7*, 1738−1748.
(18) Choi, S. H.; Kang, Y. C. Kilogram-Scale Production of SnO_2 Yolk-Shell Powders by a Spray-Drying Process Using Dextrin as Carbon Source and Drying Additive. *Chem.—Eur. J.* **2014**, *20*, 5835−5839.
(19) Li, W.-Y.; Xu, L.-N.; Chen, J. Co_3O_4 Nanomaterials in Lithium-Ion Batteries and Gas Sensors. *Adv. Funct. Mater.* **2005**, *15*, 851−857.
(20) Sun, C.; Rajasekhara, S.; Chen, Y.; Goodenough, J. B. Facile Synthesis of Monodisperse Porous Co_3O_4 Microspheres with Superior Ethanol Sensing Properties. *Chem. Commun.* **2011**, *47*, 12852−12854.
(21) Wen, Z.; Zhu, L.; Mei, W.; Li, Y.; Hu, L.; Sun, L.; Wan, W.; Ye, Z. A Facile Fluorine-Mediated Hydrothermal Route to Controlled Synthesis of Rhombus-Shaped Co_3O_4 Nanorod Arrays and Their Application in Gas Sensing. *J. Mater. Chem.* **2013**, *1*, 7511−7518.
(22) Kolmakov, A.; Klenov, D. O.; Lilach, Y.; Stemmer, S.; Moskovits, M. Enhanced Gas Sensing by Individual SnO_2 Nanowires and Nanobelts Functionalized with Pd Catalyst Particles. *Nano Lett.* **2005**, *5*, 667−673.
(23) Chan, M. Y.; Zhao, M.; Huang, J.; Au, K.; Wong, M. H.; Yao, H. M.; Lu, W.; Chen, Y.; Ong, C. W.; Chan, H. L. W.; Dai, J. Highly Sensitive Gas Sensor by the $LaAlO_3/SrTiO_3$ Heterostructure with Pd Nanoparticle Surface Modulation. *Adv. Mater.* **2014**, *26*, 5962−5968.
(24) Yang, D.-J.; Kamienchick, I.; Youn, D. Y.; Rothschild, A.; Kim, I.-D. Ultrasensitive and Highly Selective Gas Sensors Based on Electrospun SnO_2 Nanofibers Modified by Pd Loading. *Adv. Funct. Mater.* **2010**, *20*, 4258−4264.
(25) Hwang, S.-J.; Choi, K.-I.; Yoon, J.-W.; Kang, Y. C.; Lee, J.-H. Pure and Pd-Loaded Co_3O_4 Hollow Hierarchical Nanostructures with Giant and Ultraselective Chemiresistivity to Xylene and Toluene. *Chem.—Eur. J.* **2015**, *21*, 5872−5878.
(26) Choi, S. H.; Kang, Y. C. One-Pot Facile Synthesis of Janus-structured SnO_2-CuO Composite Nanorods and Their Application as Anode Materials in Li-Ion Batteries. *Nanoscale* **2013**, *5*, 4662−4668.
(27) Choi, S. H.; Kang, Y. C. Ultrafast Synthesis of Yolk-Shell and Cubic NiO Nanopowders and Application in Lithium Ion Batteries. *ACS Appl. Mater. Interfaces* **2014**, *6*, 2312−2316.
(28) Choi, J.-K.; Hwang, I.-S.; Kim, S.-J.; Park, S.-S.; Jeong, U.; Kang, Y. C.; Lee, J.-H. Design of Selective Gas Sensors Using Electrospun Pd-Doped SnO_2 Hollow Nanofibers. *Sens. Actuators, B* **2010**, *150*, 191−199.
(29) Mclntyre, N. S.; Cook, M. G. X-ray Photoelectron Studies on Some Oxides and Hydroxides of Cobalt, Nickel, and Copper. *Anal. Chem.* **1975**, *47*, 2208−2213.
(30) Barr, T. L. An ESCA Study of the Termination of the Passivation of Elemental Metals. *J. Phys. Chem.* **1978**, *82*, 1801−1810.
(31) Barr, T. L. Recent Advances in Xray Photoelectron Spectroscopy Studies of Oxides. *J. Vac. Sci. Technol. A* **1991**, *9*, 1793−1805.
(32) Armelao, L.; Barreca, D.; Gross, S.; Tondello, E. Sol-Gel and CVD Co_3O_4 Thin Films Characterized by XPS. *Surf. Sci. Spectra* **2001**, *8*, 14−23.
(33) Kim, H.-J.; Lee, J.-H. Highly Sensitive and Selective Gas Sensors Using P-type Oxide Semiconductors: Overview. *Sens. Actuators B* **2014**, *192*, 607−627.
(34) Jeong, H.-M.; Kim, H.-J.; Rai, P.; Yoon, J.-W.; Lee, J.-H. Cr-Doped Co_3O_4 Nanorods as Chemiresistor for Ultraselective Monitoring Methyl Benzene. *Sens. Actuators, B* **2014**, *201*, 482−489.
(35) Yamazoe, New Approaches for Improving Semiconductor Gas Sensors. *Sens. Actuators, B* **1991**, *5*, 7−19.
(36) Brezinsky, K. The High-Temperature Oxidation of Aromatic Hydrocarbons. *Prog. Energy Combust. Sci.* **1986**, *12*, 1−24.
(37) Kanda, K.; Maekawa, T. Development of a WO_3 Thick-Film-Based Sensor for the Detection of VOC. *Sens. Actuators, B* **2005**, *108*, 97−101.
(38) Occupational Safety & Health Administration. http://www.osha.gov (accessed Nov 7, 2014).
(39) Li, K.-M.; Li, Y.-J.; Lu, M.-Y.; Kuo, C.-I.; Chen, L.-J. Direct Conversion of Single-layer SnO Nanoplates to Multi-layer SnO_2 Nanoplates with Enhanced Ethanol Sensing Properties. *Adv. Funct. Mater.* **2009**, *19*, 2453−2456.
(40) Jing, Z.; Zhan, J. Fabrication and Gas-sensing Properties of Porous ZnO Nanoplates. *Adv. Mater.* **2008**, *20*, 4547−4551.
(41) Moon, H. G.; Shim, Y.-S.; Kim, D. H.; Jeong, H. Y.; Jeong, M.; Jung, J. Y.; Han, S. M.; Kim, J. K.; Kim, J.-S.; Park, H.-H.; Lee, J.-H.; Tuller, H. L.; Yoon, S.-J.; Jang, H. W. Self-activated Ultrahigh Chemosensitivity of Oxide Thin Film Nanostructures for Transparent Sensors. *Sci. Rep.* **2012**, *2*, 588.

DOI: 10.1021/acsami.5b00706
ACS Appl. Mater. Interfaces 2015, 7, 7717−7723